Biochemical Pharmacology 83 (2012) 1159–1171

Contents lists available at SciVerse ScienceDirect

Biochemical Pharmacology

journal homepage: www.elsevier.com/locate/biochempharm

Vinca alkaloids cause aberrant ROS-mediated JNK activation, Mcl-1 downregulation, DNA damage, mitochondrial dysfunction, and apoptosis in lung adenocarcinoma cells

Wei-Hsin Chiu [a,b], Sheng-Jei Luo [a], Chia-Ling Chen [c], Jai-Hong Cheng [d], Chia-Yuan Hsieh [a], Chi-Yun Wang [a,e], Wei-Ching Huang [a], Wu-Chou Su [a,b,e,*], Chiou-Feng Lin [a,c,e,f,*]

[a] Institute of Clinical Medicine, College of Medicine, National Cheng Kung University, Tainan, Taiwan
[b] Division of Hemato-Oncology, Department of Internal Medicine, National Cheng Kung University Hospital, College of Medicine, National Cheng Kung University, Tainan, Taiwan
[c] Center of Infectious Disease and Signaling Research, College of Medicine, National Cheng Kung University, Tainan, Taiwan
[d] Department of Pediatrics, Chang Gung Memorial Hospital-Kaohsiung Medical Center, Kaohsiung, Taiwan
[e] Institute of Basic Medical Sciences, College of Medicine, National Cheng Kung University, Tainan, Taiwan
[f] Department of Microbiology and Immunology, College of Medicine, National Cheng Kung University, Tainan, Taiwan

ARTICLE INFO

Article history:
Received 10 November 2011
Accepted 12 January 2012
Available online 20 January 2012

Keywords:
Vinca alkaloids
Lung adenocarcinoma
Mitotic arrest
Apoptosis
ROS
JNK
Mcl-1
Mitochondria
Caspase

ABSTRACT

Vinca alkaloids are clinically used to inhibit the growth of malignancy by interfering with microtubule polymerization. The purpose of this study was to identify the molecular mechanisms underlying growth inhibition as well as apoptosis in vinca alkaloid-treated lung adenocarcinoma cells. Consistent with nocodazole, treatment with vinorelbine (VNR) caused mitotic prometaphase arrest in a time-dependent manner, accompanied by cell apoptosis, dependent on both dose and time. VNR sequentially induced mitochondrial transmembrane potential (MTP) loss and caspase-dependent apoptosis following myeloid cell leukemia (Mcl) 1 downregulation. Prolonged activation of c-Jun N-terminal kinase (JNK) was required for vinca alkaloid- and nocodazole-induced apoptosis but not cell cycle arrest. Vinca alkaloids and nocodazole caused glutathione/reactive oxygen species (ROS) imbalance, and inhibiting ROS prevented prolonged JNK activation, decreased Mcl-1 levels, MTP loss, and apoptosis. Notably, cell size and granularity were enlarged in stimulated cells; unexpectedly, many ROS-producing mitochondria were accumulated followed by aberrant JNK-mediated mitochondrial dysfunction. Unlike cisplatin, which causes DNA damage in each phase of the cell cycle, VNR and nocodazole induced aberrant JNK-regulated DNA damage in prometaphase; however, inhibiting ATM (ataxia telangiectasia, mutated) and ATR (ATM and Rad3-related) did not reverse mitotic arrest or apoptosis. These results demonstrate an essential role of ROS in vinca alkaloid-induced aberrant JNK-mediated Mcl-1 downregulation and DNA damage followed by mitochondrial dysfunction-related apoptosis but not mitotic arrest.

1. Introduction

Lung cancer is one of the leading causes of death worldwide. In 2010, there were approximately 222,520 newly diagnosed cases and 157,300 deaths from lung and bronchus cancer in the United States [1]. Many chemotherapy agents have shown therapeutic benefits in lung cancer, e.g., microtubule inhibitors (taxenes and vinca alkaloids), antimetabolites (pemetrexed and gemcitabine), etc. Vinca alkaloids, including vinorelbine (VNR), vincristine, vinblastine, and vindesine, bind to tubulin as potent inhibitors of mitotic microtubule polymerization. VNR, a semi-synthetic vinca alkaloid, is used both as a single agent and in combination with cisplatin for first-line treatment of advanced and metastatic non-small cell lung cancer (NSCLC). The lipophilic feature ensures that VNR is rapidly distributed over the peripheral tissues, so the peak plasma concentration of VNR is about 1 μM. The levels decay to 100 nM at 1 h and to 10 nM at 24 h after the intravenous infusion of 20–30 mg/m^2 [2,3]. The concentration of VNR that is used in *in vitro* studies is thought to be equal to the levels in plasma [4].

In addition to causing cell cycle arrest by targeting microtubules, VNR causes apoptosis of leukemia and lymphoma cells

* Corresponding authors at: Institute of Clinical Medicine, College of Medicine, National Cheng Kung University, Tainan, Taiwan. Tel.: +886 6 2353535x4240; fax: +886 6 2758781.
E-mail addresses: wei_hsin2005@yahoo.com.tw (W.-H. Chiu), losnja2001@yahoo.com.tw (S.-J. Luo), clchen2001.tw@yahoo.com.tw (C.-L. Chen), cjaiho@yahoo.com.tw (J.-H. Cheng), dyoushus@yahoo.com.tw (C.-Y. Hsieh), chixuan1225@hotmail.com (C.-Y. Wang), zarbi@mail2000.com.tw (W.-C. Huang), Sunnysu@mail.ncku.edu.tw (W.-C. Su), cflin@mail.ncku.edu.tw (C.-F. Lin).

0006-2952/$ – see front matter © 2012 Elsevier Inc. All rights reserved.
doi:10.1016/j.bcp.2012.01.016

through caspase-3 activation [5]. Combination treatment of vinca alkaloids and paclitaxel induces apoptosis with caspase-8 activation, independent of CD95 in human colon cancer cells [6]. Phosphorylated Bcl-2 and activated caspase-8, -9, and -3 are observed in tumor tissues of NSCLC patients with VNR treatment [7]. VNR causes apoptosis by increasing Bax and Bcl-xs expression, decreasing Bcl-2 and Bcl-xL, releasing cytochrome *c*, and augmenting caspase-9 and caspase-3 activities in lung carcinoma cells [8]. Furthermore, VNR-induced apoptosis is enhanced by the activation of caspase-8 via caspase-9-mediated activation of caspase-3 but not through CD95 in Jurkat cells [9]. Therefore, an intrinsic pathway of mitochondrial dysfunction-related apoptosis is usually induced by VNR.

Myeloid cell leukemia (Mcl) 1 localizes in the mitochondria, promotes cell survival by suppressing cytochrome *c* release from mitochondria and is regulated at the transcriptional and post-translational levels. The mitogen-activated protein kinase c-Jun N-terminal kinase (JNK) phosphorylates Ser121 and Thr163 of Mcl-1 and then induces Mcl-1 inactivation after stimulation with hydrogen peroxide [10]. Mcl-1 is rapidly degraded through two main routes by caspase-mediated and proteasome-dependent degradation. Activation of caspase-3 cleaves Mcl-1 at Asp127 and Asp157 to expose a C-terminal domain with a death-promoting activity [11,12]. Additionally, glycogen synthase kinase-3 causes Ser159 and Thr163 phosphorylation to facilitate Mcl-1 ubiquitylation and degradation in response to apoptotic stimuli [13]. Vinblastine induces JNK-mediated phosphorylation and the consequent inactivation of Bcl-2 and Bcl-xL prior to caspase-3 activation [14]. However, the molecular basis for JNK activation remains unknown.

Oxidative stress-activated apoptosis signal regulating kinase 1/JNK is important for apoptosis [15]. Chemotherapy, radiotherapy, and photodynamic therapy can often promote reactive oxygen species (ROS) generation while killing tumor cells by the generation of ROS directly in tumor cells or by inhibiting the anti-oxidative enzymes of tumor cells [16]. VNR can cause vascular toxicities. Notably, it has been demonstrated that VNR induces oxidative stress by increasing ROS generation to cause depolarization of mitochondrial membranes in porcine aorta endothelial cells [4]. However, the oxidative stress caused by VNR lacks a mechanism study. In this study, we demonstrated an essential role of ROS in vinca alkaloid-induced aberrant JNK-mediated Mcl-1 downregulation followed by mitochondrial dysfunction and apoptosis in lung adenocarcinoma cells. We further examined a possible mechanism for ROS generation caused by VNR. The effects of aberrant ROS/JNK on vinca alkaloid-induced mitotic arrest and DNA damage were also investigated.

2. Materials and methods

2.1. Drugs

VNR was purchased from Sigma–Aldrich (St. Louis, MO). The broad-spectrum caspase inhibitor, benzyloxycarbonyl-Val-Ala-Asp(O-Me)-fluoro methyl ketone (z-VAD-fmk), caspase-3 inhibitor benzyloxycarbonyl-Asp(O-Me)-Glu(O-Me)-Val-Asp(O-Me)-fluoromethyl ketone (z-DEVD-fmk), caspase-9 inhibitor benzyloxycarbonyl-Leu-Glu(O-Me)-His-Asp(O-Me)-fluoromethyl ketone (z-LEHD-fmk), and caspase-2 inhibitor benzyloxycarbonyl-Val-Asp(O-Me)-Val-Ala-Asp(O-Me)-fluoromethyl ketone (z-VDVAD-fmk) were also purchased from Sigma–Aldrich and dissolved in dimethyl sulfoxide (DMSO). Nocodazole, cathepsin B inhibitor benzyloxycarbonyl-Phe-Ala-fluoromethyl ketone (z-FA-fmk), cathepsin D inhibitor pepstatin A, GSK-3 inhibitors lithium chloride (LiCl), 6-bromoindirubin-3′-oxime (BIO), SB216763, and SB415286, proteasome inhibitor MG132, and ATM (ataxia telangiectasia, mutated) and ATR (ATM and Rad3-related) inhibitor caffeine were purchased from Calbiochem (San Diego, CA). MEK inhibitor PD98059, JNK inhibitor SP600125, p38 MAPK inhibitor SB202190, and antioxidant diphenylene iodonium (DPI) were obtained from Sigma–Aldrich and dissolved in DMSO prior to dilution with PBS. Rabbit anti-human MPM2, α-tubulin, lamin A/C, PARP, caspase-3, Bcl-2, Mcl-1, Bcl-xL, phospho-apoptosis signal regulating kinase (ASK) 1 (Thr845), ASK1, phospho-JNK (Thr183/Tyr185), JNK, and γ-H2AX were purchased from Cell Signaling Technology (Beverly, MA). β-actin antibodies and horseradish peroxidase-conjugated anti-rabbit IgG were obtained from Chemicon International (Temecula, CA). All drug treatments in cells were assessed for their cytotoxic effects using cytotoxicity assays before experiments. Non-cytotoxic dosages were used in this study.

2.2. Cell culture

Human lung adenocarcinoma AS2 cell line was established from ascites that had been generated by PC14PE6 cells (a gift from Isaiah J. Fidler) (MD Anderson Cancer Center, Houston, TX) in nude mice [17]. AS2 and human lung adenocarcinoma A549 cells were routinely grown on plastic in Dulbecco's modified Eagle's medium (Gibco-BRL; Grand Island, NY) with L-glutamine and 15 mM HEPES, supplemented with 10% fetal bovine serum (Gibco-BRL), 100 units of penicillin, and 100 μg/ml streptomycin and maintained at 37 °C in 5% CO_2. Other chemical drugs used for cell culture were purchased from Sigma–Aldrich.

2.3. Cytotoxicity assay

To evaluate cell damage, lactate dehydrogenase (LDH) activity was assayed using a colorimetric assay (Cytotoxicity Detection kit; Roche Diagnostics, Lewes, UK) according to the manufacturer's instructions. Aliquots of the culture media were transferred to 96-well microplates. A microplate reader (Spectra MAX 340PC; Molecular Devices, Sunnyvale, CA) was used to measure the absorbance at 620 nm with a reference wavelength of 450 nm, and the data were analyzed with Softmax Pro software.

2.4. Cell cycle and apoptosis assay

The cell cycle and apoptosis was analyzed using nuclear propidium iodide (PI; Sigma–Aldrich) staining as previously described [18] and then analyzed using flow cytometry (FACSCalibur; Becton Dickinson, San Jose, CA) with excitation set at 488 nm and emission detected at the FL-2 channel (565–610 nm). For cell cycle analysis, the distribution of cells in different phases of the cell cycle was calculated using the MetaMorph software (Molecular Devices, Downingtown, PA). For apoptotic analysis, the samples were analyzed using CellQuest Pro 4.0.2 software (Becton Dickinson), and quantification was performed using WinMDI 2.8 software (The Scripps Institute, La Jolla, CA). Apoptosis levels were reported as percentages of sub-G_1. Annexin V plus PI staining was also performed using a commercial kit (Sigma–Aldrich) according to the manufacturer's instructions. To observe nuclear condensation, 4′,6-diamidino-2-phenylindole (DAPI; Sigma–Aldrich)-stained cells were observed using a fluorescence microscope (IX71; Olympus, Tokyo, Japan).

2.5. Immunostaining

The cells were fixed in 3.7% formaldehyde (Sigma–Aldrich) in PBS for 10 min. After washing twice with PBS, the cells were incubated with primary antibodies against MPM2, α-tubulin, lamin A/C, phospho-JNK, and γ-H2AX in antibody diluent (DAKO Corporation, Carpinteria, CA) with or without PI for DNA content

staining and incubated at 4 °C overnight. The next day, the samples were washed with PBS and then incubated with or without Alexa Fluor 488- or 594-labeled secondary antibodies at room temperature for 1 h. The samples were acquired with FACSCalibur with excitation set at 488 and 633 nm; emission was detected using the FL-1 (515–545 nm) and FL-2 (565–610 nm) channels. The samples were analyzed using CellQuest Pro 4.0.2 software, and quantification was performed using WinMDI 2.8 software. For confocal observation, the cells were washed with PBS and visualized under a laser-scanning confocal microscope (SPII; Leica Mikrosysteme Vertrieb GmbH, Bensheim, Germany). DAPI (1:200) was added for nuclear counter-staining and was applied at room temperature for 10 min. For annexin V plus MPM2 co-staining, cells were stained with annexin V using a commercial kit (Sigma–Aldrich) according to the manufacturer's instructions. Cells were then fixed in 3.7% formaldehyde in PBS for 10 min. After washing twice with PBS, the cells were incubated with primary antibodies against MPM2 and secondary antibody and then visualized under a laser-scanning confocal microscope (SPII).

2.6. Western blotting

Harvested cells were lysed with a buffer containing 1% Triton X-100, 50 mM of Tris (pH 7.5), 10 mM of EDTA, 0.02% NaN_3, and a protease inhibitor cocktail (Roche Boehringer Mannheim Diagnostics, Mannheim, Germany). Following one cycle of freeze–thaw, cell lysates were centrifuged at 10,000 × *g* at 4 °C for 20 min. Lysates were boiled in sample buffer for 5 min. The proteins were then subjected to SDS-PAGE and transferred to PVDF membrane (Millipore, Billerica, MA) using a semi-dry electroblotting system. After blocking with 5% skim milk in PBS, the membranes were incubated with a 1/1000 dilution of primary antibodies at 4 °C overnight. The membranes were then washed with 0.05% PBS-Tween 20 and incubated with a 1/5000 dilution of horseradish peroxidase-conjugated secondary antibodies at room temperature for 1 h. After washing, the membranes were soaked in ECL solution (PerkinElmer Life Sciences Inc., Boston, MA) for 1 min, and then exposed to film (BioMax; Eastman Kodak, Rochester, NY). Other chemical drugs used for protein assay were purchased from Sigma–Aldrich.

2.7. Mitochondrial functional assay

To evaluate mitochondrial damage, the loss of mitochondria transmembrane potential (MTP) was assayed by rhodamine 123 (Sigma–Aldrich) and then analyzed using flow cytometry (FACSCalibur) with excitation set at 488 nm; emission was detected with the FL-1 channel (515–545 nm). Samples were analyzed using CellQuest Pro 4.0.2 software, and quantification was done using WinMDI 2.8 software. Small cell debris was excluded by gating on a forward scatter plot.

2.8. RT-PCR

Total cellular RNA was extracted using an Ultraspec-II RNA isolation system (Biotecx, Houston, TX, USA) following the manufacturer's instructions. The concentration of RNA was quantified by spectrophotometry at 260 nm (U-2000; Hitachi, Tokyo, Japan). The cDNA, in a total volume of 100 μl, was prepared after reverse transcription of cellular RNA (20 μg) with Moloney murine leukemia virus reverse transcriptase (Promega, Madison, WI) using an 18-mer oligo(dT) as the primer. The cDNA (3 μl) was added to the PCR buffer containing primers (1.5 μM each), $MgCl_2$ (1.5 mM), dNTPs (0.2 mM each), and *Taq* DNA polymerase (1 U; Promega) in a total reaction volume of 50 μl. Oligonucleotide primers for human Mcl-1 (5′-AGACCTTACGACGGGTTGG-3′ and 5′-AATCCTGCCCCAGTTTGTT-3′) and β-actin (5′-CTCCTTAATGTCACGCACGAT-3′ and 5′-CATGTACGTTGCTATCCAGGC-3′) were used. Thirty cycles were performed (95 °C for 1 min, 55 °C for 2 min, and 72 °C for 3 min) using a PCR controller (GeneAmp PCR System 2400; PerkinElmer, Wellesley, MA). The PCR products were separated by 1.5% agarose gel electrophoresis, stained with ethidium bromide, and viewed with UV light. Other chemical drugs used for RT-PCR were purchased from Sigma–Aldrich.

2.9. GSH detection

Cellular glutathione (GSH) was assayed using the ApoAlert Glutathione Detection kit (Clontech, Palo Alto, CA) according to the manufacturer's instructions. The cells were detected with the FL-1 channel (515–545 nm) by FACSCalibur. The mean fluorescent intensity (MFI) was analyzed using CellQuest Pro 4.0.2 software, and quantification was performed using WinMDI 2.8 software.

2.10. Intracellular ROS assay

Intracellular oxidative stress was measured by dichlorodihydrofluorescein diacetate oxidation. Cells were exposed to 20 μM 5-(and-6)-chloromethyl-2′,7′-dichlorodihydrofluorescein diacetate, acetyl ester (CM-H_2DCFDA) (Invitrogen, San Diego, CA) for 1 h. The cells were detected with the FL-1 channel (515–545 nm) by FACSCalibur. The MFI was analyzed using CellQuest Pro 4.0.2 software, and quantification was done using WinMDI 2.8 software. Small cell debris was excluded by gating on a forward scatter plot. For CM-H_2DCFDA plus MPM2 co-staining, cells were stained with CM-H_2DCFDA as described above and then fixed in 3.7% formaldehyde in PBS for 10 min. After washing twice with PBS, the cells were incubated with primary antibodies against MPM2 and secondary antibody and then visualized under a laser-scanning confocal microscope (SPII).

2.11. Mitochondria and mitochondrial ROS detection

To detect mitochondria, the cells were dyed with 200 nM MitoTracker Green (Invitrogen) for 30 min at 37 °C, according to the manufacturer's instructions, and analyzed using flow cytometry (FACSCalibur) with excitation set at 488 nm. For detecting mitochondrial ROS, the cells were dyed with 200 nM MitoSOX Red (Invitrogen) for 30 min at 37 °C according to the manufacturer's instructions. After another washing with PBS, the cells were also analyzed using flow cytometry (FACSCalibur) with excitation set at 488 nm. The MFI was analyzed using CellQuest Pro 4.0.2 software, and quantification was performed using WinMDI 2.8 software.

2.12. Mitochondrial dysfunction detection

XF24 Extracellular Flux Analyzer (Seahorse Bioscience, Billerica, MA) was used to evaluate VNR-induced mitochondrial toxicity by monitoring oxygen consumption rate (OCR) and the extracellular acidification rate (ECAR) [19]. The levels of OCR and ECAR of VNR-treated AS2 cells were monitored in a 24-well plate format using a phosphorescent oxygen- and hydrogen-sensitive probe, according to the manufacturer's instructions. Time profiles of fluorescence intensity in each well were analyzed using XF software algorithm and Excel (Microsoft software, Redmond, WA).

2.13. Statistical analysis

Values are expressed as means ± standard deviation (SD). Groups were compared using Student's two-tailed unpaired *t* test or one-way ANOVA analysis followed by Dunnet's post hoc test, as appropriate. Statistical significance was set at $P < 0.05$.

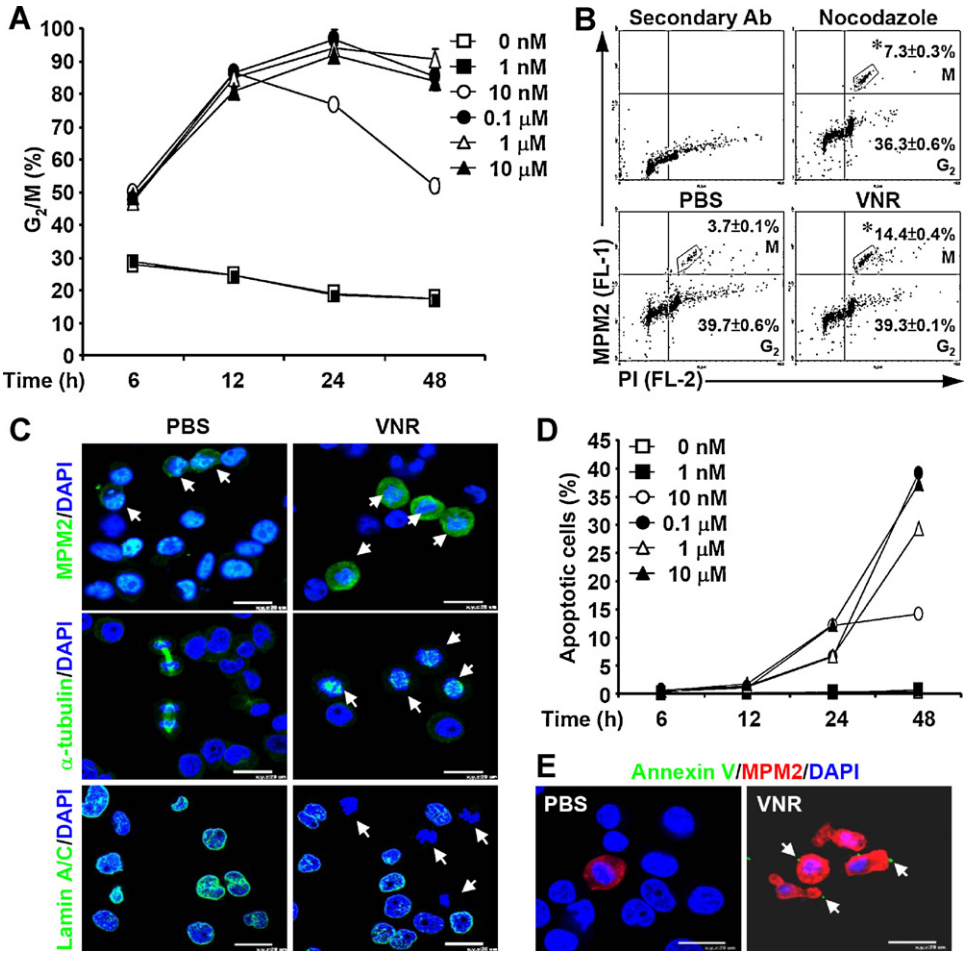

Fig. 1. VNR causes mitotic prometaphase arrest and apoptosis in human lung adenocarcinoma cells. (A) Nuclear PI staining and flow cytometric analysis were used to determine the cell cycle stage of AS2 cells treated with VNR at the indicated dose and time. (B) Mitotic phase cells were determined by analysis of DNA content (PI staining) and MPM2 staining followed by flow cytometric analysis after 6 h post-treatment of VNR (5 nM). Treatment of nocodazole (40 ng/ml) was used as a positive control. The data are the means ± SD of three individual experiments; $^{*}P < 0.05$, compared with PBS-treated group. (C) Immunostaining and subsequent fluorescent microscopy were used to determine the expression patterns of MPM2, α-tubulin, and lamin A/C in VNR (5 nM)-treated AS2 cells for 6 h. DAPI was used for nuclear staining. One representative image obtained from three individual experiments is shown. Scale bar is 25 μm. (D) Nuclear PI staining and subsequent flow cytometric analysis were used to determine VNR-induced apoptosis in AS2 cells in a dose- and time-dependent manner. For flow cytometric analysis, the percentages of G_2/M phase cells and apoptotic cells at sub-G_1 phase are shown as the means ± SD from three individual experiments. (E) Annexin V plus MPM2 staining followed by fluorescent microscopic observations were used to determine apoptosis in mitotic phase cells without or with VNR (1 μM) treatment for 24 h. One representative image obtained from three individual experiments is shown. Scale bar is 25 μm.

3. Results

3.1. VNR-induced arrest at mitotic prometaphase and apoptosis

VNR causes cellular cytotoxicity via cell cycle arrest followed by apoptosis [5]. In this study, we investigated the molecular basis of VNR in cell cycle progression and cytotoxicity in AS2 human lung adenocarcinoma cells. The dose responses and time kinetics of VNR-induced cell cycle arrest at the G_2/M phase in these cells were shown using nuclear PI staining followed by flow cytometric analysis ($P < 0.05$, Fig. 1A). To further characterize the specific phase arrest caused by VNR, the increased expression of MPM2, a mitotic phase marker [20], was determined using flow cytometry. Consistent with nocodazole, a positive control for causing prometaphase arrest [21], VNR significantly ($P < 0.05$) enhanced the expression of MPM2 as compared with PBS-treated group, indicating the effects of VNR specifically on cell cycle arrest at the mitotic phase but not the G_2 phase (Fig. 1B). Image of immunostaining showed that VNR caused MPM2 increase (Fig. 1C). Furthermore, immunostaining using α-tubulin and lamin A/C antibodies demonstrated that VNR caused mitotic prometaphase arrest due to the constitutive lack of α-tubulin rearrangement and the presence of lamin A/C degradation (Fig. 1C). The analyses of nuclear PI staining followed by flow cytometric analysis showed that VNR significantly ($P < 0.05$) caused AS2 cells to undergo apoptosis in a time- and dose-dependent manner (Fig. 1D). Annexin V plus PI staining confirmed this result by characterizing the presence of phosphatidylserine externalization only in non-fixed VNR-treated AS2 cells (data not shown). Notably, inconsistent with mitotic phase cells presenting in normal culture condition, annexin V plus MPM2 co-staining confirmed that AS2 cells underwent apoptosis following mitotic arrest caused by VNR (Fig. 1E). These results show that VNR induces arrest at mitotic prometaphase accompanied by apoptosis in human lung adenocarcinoma cells.

3.2. VNR-induced MTP loss and caspase-dependent apoptosis

Dysregulation of intracellular organelles and activation of the caspase cascade are generally involved in cell apoptosis [22]. Using PI staining followed by flow cytometric analysis, we found that treatment with the pan-caspase inhibitor z-VAD-fmk (Fig. 2A and Supplemental Fig. S1), the caspase-3 inhibitor z-DEVD-fmk, and the caspase-9 inhibitor z-LEHD-fmk (Fig. 2B) effectively ($P < 0.05$)

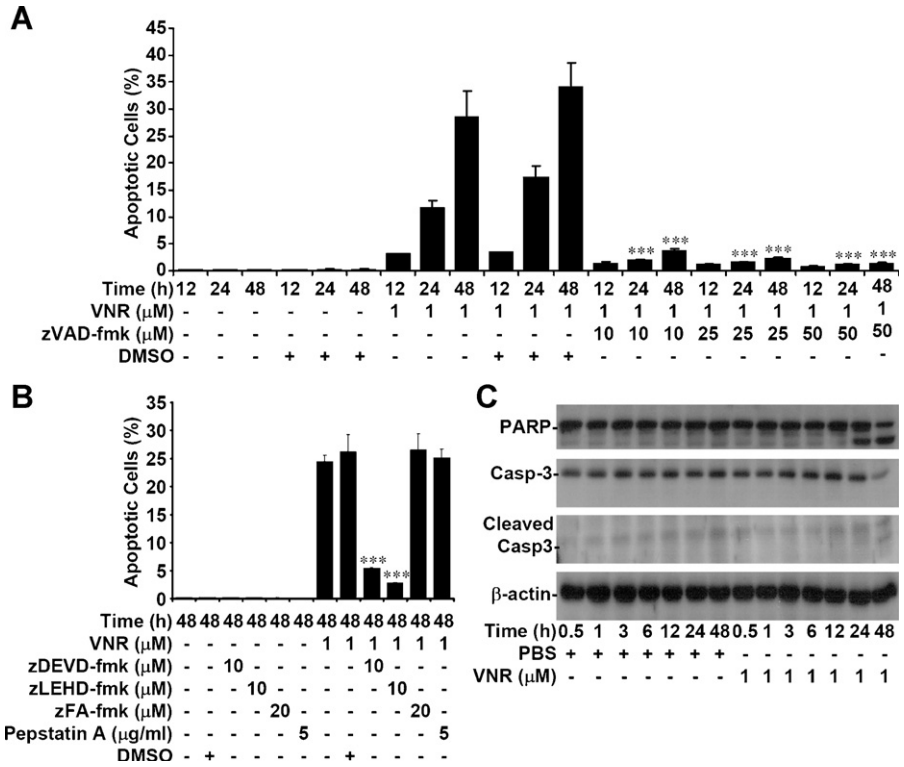

Fig. 2. VNR induces caspase-dependent cell apoptosis. AS2 cells were pretreated with the pan-caspase inhibitor z-VAD-fmk (A), the caspase-3 inhibitor z-DEVD-fmk, the caspase-9 inhibitor z-LEHD-fmk, the cathepsin B inhibitor z-FA-fmk, or the cathepsin D inhibitor pepstatin A (B) for 0.5 h followed by VNR or PBS treatment for the indicated time. DMSO was used as a negative control. PI staining followed by flow cytometric analysis was used to determine the induction of cell apoptosis. The data are means ± SD of three experiments; ***$P < 0.001$, compared with the VNR-treated group. (C) Western blotting was used to determine the expression of PARP and cleaved caspase-3 (Casp3) in VNR-treated AS2 cells for the indicated time. β-actin was used as an internal control. One representative dataset obtained from repeated experiments is shown.

blocked VNR-induced apoptosis in AS2 cells. Western blotting confirmed that VNR caused caspase-3 activation and PARP cleavage, suggesting the apoptotic effects of VNR treatment (Fig. 2C). To investigate the involvement of dysfunction on intracellular organelles, such as mitochondria and lysosomes, lysosomal cathepsin inhibitors (z-FA-fmk for cathepsin B and pepstatin A for cathepsin D) were first applied. The results showed that inhibiting cathepsin B or D did not block the apoptotic effects of VNR (Fig. 2B), suggesting a lysosome-independent apoptotic pathway caused by VNR.

We next investigated the molecular mechanisms of VNR-induced mitochondrial dysfunction. The time kinetics of VNR-induced loss of MTP in AS2 cells were shown by lipophilic cationic fluorochrome rhodamine 123 staining followed by flow cytometric analysis ($P < 0.05$, Fig. 3A). Bcl-2 family proteins are important for controlling mitochondrial function [23]. We investigated the effects of VNR on the expression of Bcl-2 family proteins, including the anti-apoptotic proteins Mcl-1, Bcl-2, and Bcl-xL in AS2 cells. Upon VNR treatment in AS2 cells, Western blot analysis showed that VNR caused a decrease in Mcl-1 expression (Fig. 3B). However, the involvement of GSK-3- (Fig. 3C), proteasome- (Fig. 3D), and caspase-mediated (Fig. 3E) Mcl-1 degradation was precluded using pharmacological approaches, while both of these factors are involved in Mcl-1 stability [12,13]. Additionally, RT-PCR assays showed that VNR did not inhibit the mRNA expression of Mcl-1 in AS2 cells (Fig. 3F). These results demonstrate that VNR induces Mcl-1 downregulation through an unknown mechanism and causes mitochondrial dysfunction followed by caspase-dependent apoptosis.

3.3. Involvement of JNK in VNR-induced mitotic arrest and apoptosis

MAPKs are mainly affected by vinca alkaloids [14]. Thus, we examined the effects of ERK, JNK, and p38 MAPK on VNR-induced mitochondrial apoptosis in AS2 cells. Flow cytometric analysis showed that treatment with the JNK inhibitor SP600125 but not the MEK inhibitor PD98059 and p38 MAPK inhibitor SB202190 significantly ($P < 0.05$) blocked VNR-induced AS2 cell apoptosis (Fig. 4B) and MTP loss (Fig. 4C). However, inhibiting MAPKs had no effects on VNR-induced G_2/M phase arrest (Fig. 4A). Western blotting showed that VNR caused activation of ASK1 and JNK by detecting their phosphorylation at active residues (Fig. 4D). To further confirm this pathway, JNK was inhibited using SP600125, which also blocked VNR-induced apoptosis but not G_2/M phase arrest in human lung adenocarcinoma A549 cells (Fig. 4E). Next, we checked whether nocodazole also caused similar apoptotic effects due to the induction of G_2/M phase arrest. First, we determined the dose of nocodazole (25 ng/ml) that caused similar levels of G_2/M phase arrest as compared with VNR (Fig. 5A). Treatment of SP600125 significantly ($P < 0.05$) inhibited nocodazole-induced apoptosis in AS2 cells (Fig. 5B). Furthermore, immunostaining confirmed that either VNR or nocodazole induced MPM2 expression in AS2 cells with JNK activation (Fig. 5C). These results show that VNR induces prolonged JNK activation followed by aberrant JNK-regulated MTP loss and mitochondrial dysfunction-related apoptosis. However, JNK is not involved in VNR-induced cell cycle arrest.

3.4. Involvement of ROS in VNR-activated JNK and vinca alkaloid-induced apoptosis

We examined the involvement of ROS in apoptosis of vinca alkaloid-treated AS2 cells during the facilitation of ASK1/JNK activation by ROS [24]. Both VNR and nocodazole treatment decreased the intracellular levels of GSH in a time-dependent manner ($P < 0.05$, Fig. 6A). In contrast, CM-H_2DCFDA staining followed by flow cytometric analysis demonstrated that both VNR

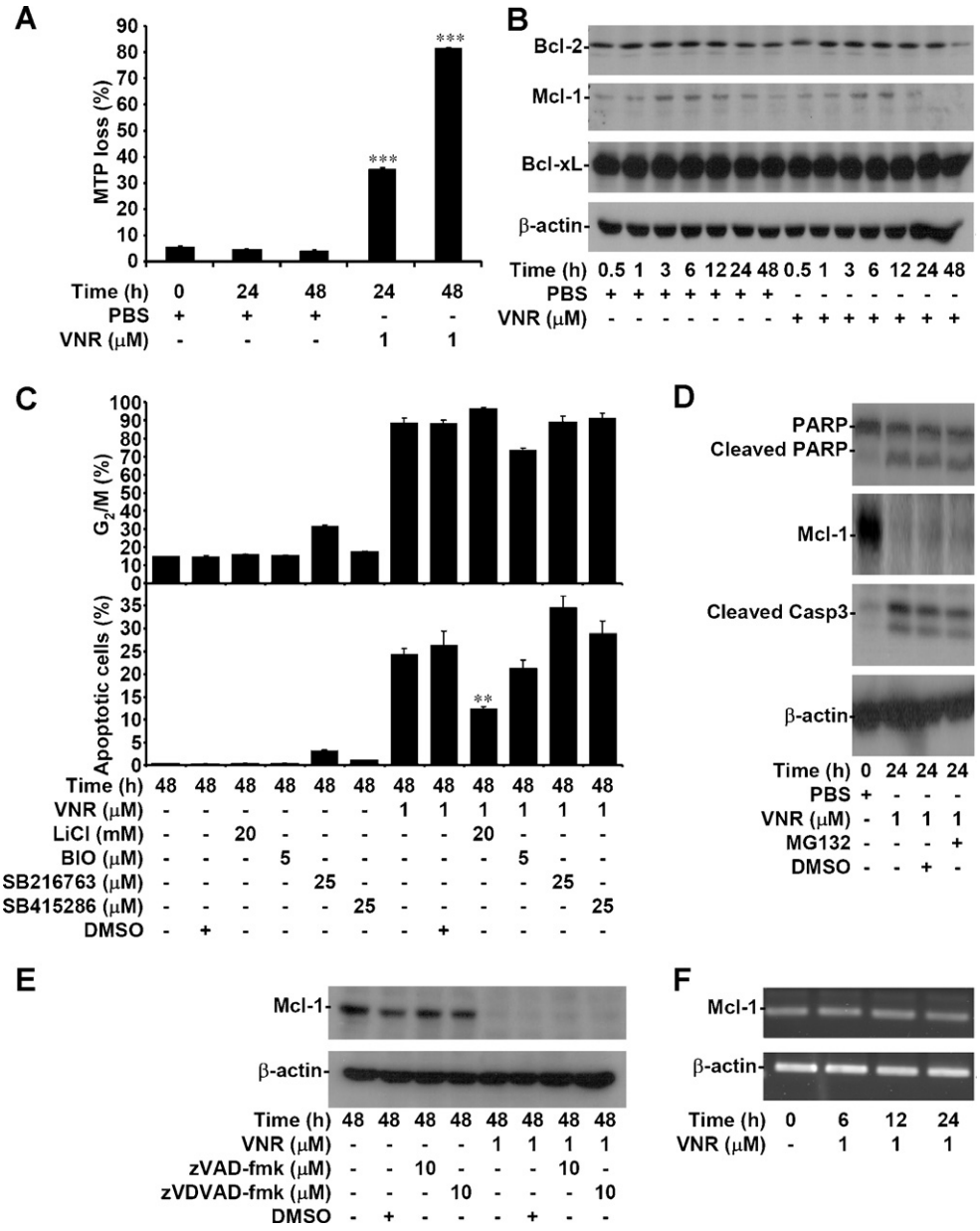

Fig. 3. VNR deregulates the expression of Bcl-2 family proteins followed by MTP loss. (A) AS2 cells were treated with VNR or PBS for the indicated time. Rhodamine 123 staining followed by flow cytometric analysis was used to determine the loss of MTP. (B) Furthermore, Western blotting was used to determine the expression of Bcl-2, Mcl-1, and Bcl-xL. (C) AS2 cells were pretreated with the GSK-3 inhibitors LiCl, BIO, SB216763, and SB415286 for 0.5 h followed by VNR or PBS treatment. PI staining followed by flow cytometric analysis was used to determine the induction of G_2/M phase arrest and cell apoptosis. DMSO was used as a negative control. For flow cytometric analysis, data are the means ± SD of three individual experiments; $^{**}P < 0.01$ and $^{***}P < 0.001$, compared with PBS- or VNR-treated group. AS2 cells were pretreated with the proteasome inhibitor MG132 (D), the pan-caspase inhibitor z-VAD-fmk, or the caspase-2 inhibitor z-VDVAD-fmk (E) for 0.5 h followed by VNR or PBS treatment. Western blotting was used to determine the expression of PARP, Mcl-1, and cleaved caspase-3 (Casp3). (F) RT-PCR was used to determine the mRNA expression of Mcl-1 in VNR-treated AS2 cells for the indicated time. For Western blotting and RT-PCR, β-actin was used as an internal control. One representative dataset obtained from repeated experiments is shown.

and nocodazole significantly ($P < 0.05$) increased the generation of intracellular ROS (Fig. 6B). To strength the oxidative effects caused by VNR, we did the similar experiments by using A549 cells. Results also confirmed that VNR significantly ($P < 0.05$) induced GSH decrease accompanied by ROS generation (Fig. 6A and B). Therefore, we hypothesized that VNR activates JNK through redox regulation. In antioxidant DPI-treated AS2 cells treated with VNR, Western blotting showed ROS-dependent JNK activation (Fig. 6C). In addition to SP600125, treatment of DPI also inhibited VNR-induced Mcl-1 downregulation, caspase-3 activation, and PARP cleavage (Fig. 6D). Using rhodamine 123 and PI staining followed by flow cytometric analysis, we found that DPI significantly ($P < 0.05$) inhibited VNR-induced MTP loss (Fig. 6E) and apoptosis (Fig. 6F) but not G_2/M phase arrest (Fig. 6G). Furthermore, inhibiting either ROS or JNK reduced vinblastine- and vincristine-induced apoptosis (Fig. 6H), indicating a common apoptotic mechanism caused by vinca alkaloids. These results demonstrate that vinca alkaloids induce ROS-regulated aberrant JNK to trigger Mcl-1 downregulation, MTP loss, and cell apoptosis.

3.5. VNR induces ROS-generating mitochondria accompanied by aberrant JNK-mediated mitochondrial dysfunction

To investigate the possible mechanisms for ROS generation, cell size and granularity were tested for the effects of VNR on mitotic inhibition. Flow cytometry analysis showed that either VNR or

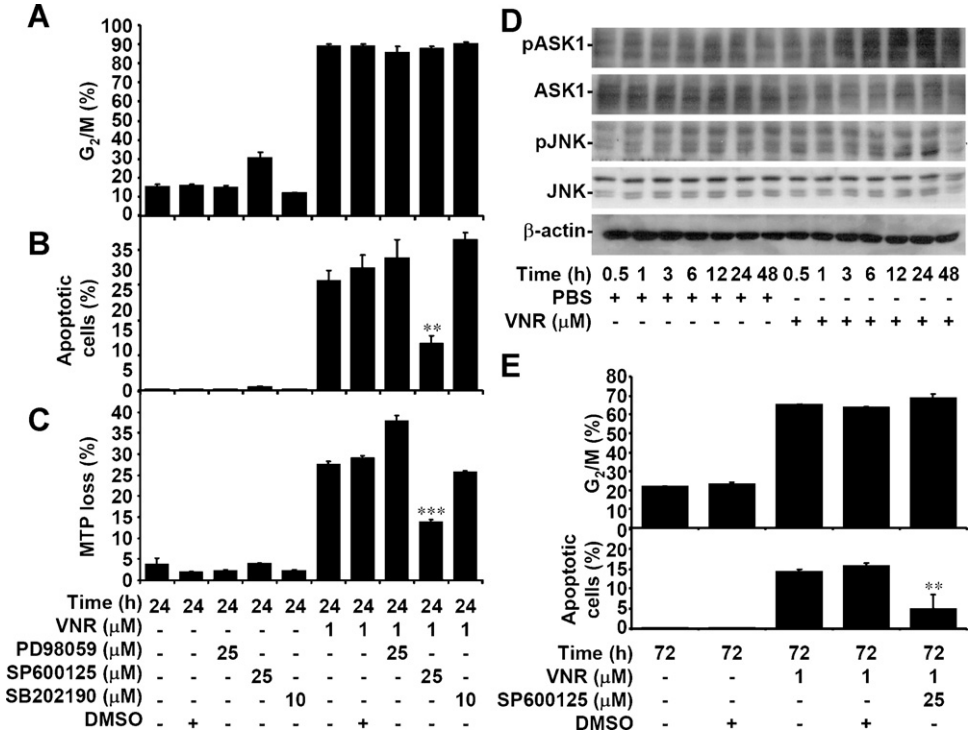

Fig. 4. VNR induces JNK-dependent Mcl-1 destabilization, MTP loss, and cell apoptosis. AS2 cells were pretreated with the MEK inhibitor PD98059, the JNK inhibitor SP600125, or the p38 MAPK inhibitor SB202190 for 0.5 h followed by VNR or PBS treatment. PI and rhodamine 123 staining followed by flow cytometric analysis were used to determine the induction of G_2/M phase arrest (A), cell apoptosis (B), and MTP loss (C). DMSO was used as a negative control. (D) Western blotting was used to determine the expression of phospho-ASK1 Thr845 (pASK1), ASK1, phospho-JNK Thr183/Tyr185 (pJNK), and JNK in VNR-treated AS2 cells for the indicated time. β-actin was used as an internal control. One representative dataset obtained from repeated experiments is shown. (E) A549 cells were pretreated with SP600125 for 0.5 h followed by VNR or PBS treatment. PI staining followed by flow cytometric analysis was used to determine the induction of G_2/M phase arrest and cell apoptosis. DMSO was used as a negative control. For flow cytometric analysis, the data are the means ± SD of three individual experiments. $^{**}P < 0.01$ and $^{***}P < 0.001$, compared with VNR-treated group.

nocodazole enlarged the size and granularity of AS2 cells (Fig. 7A). The increased cellular granularity might be the result of mitotic arrest, which causes an increase in the total amount of DNA and intracellular organelles [25]. Mito-Tracker Green staining followed by flow cytometry confirmed the increased mitochondrial expression in either VNR- or nocodazole-treated AS2 cells ($P < 0.05$, Fig. 7B). MitoSOX-stained, VNR- and nocodazole-treated AS2 cells showed a high intracellular oxidative state ($P < 0.05$, Fig. 7C). Notably, VNR considerably increased ROS generation in cells with M phase (Fig. 7D). These results indicate that VNR causes

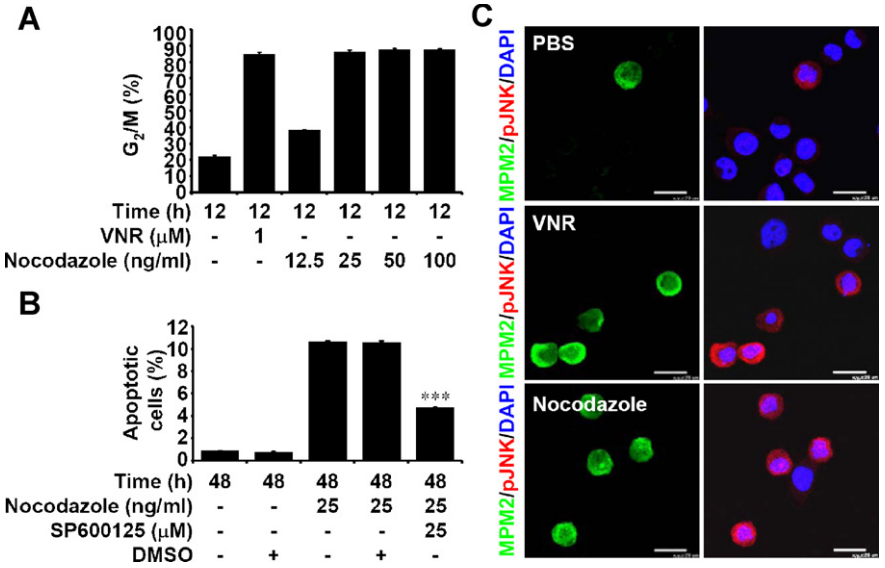

Fig. 5. Nocodazole induces JNK-regulated cell apoptosis. (A) PI staining and subsequent flow cytometric analysis were used to determine the cell cycle stage of AS2 cells treated with VNR or various doses of nocodazole. (B) AS2 cells were pretreated with SP600125 for 0.5 h followed by nocodazole or PBS treatment. PI staining followed by flow cytometric analysis was used to determine the induction of cell apoptosis. DMSO was used as a negative control. For flow cytometric analysis, the data are the means ± SD of three individual experiments; $^{***}P < 0.001$, compared with the PBS- or nocodazole-treated group. (C) Immunostaining followed by fluorescent microscopic observation was used to determine the expression of MPM2 and phospho-JNK Thr845 (pJNK) in VNR (1 μM)- or nocodazole (25 ng/ml)-treated AS2 cells for 12 h. DAPI was used for nuclear staining. One representative image obtained from three individual experiments is shown. Scale bar is 25 μm.

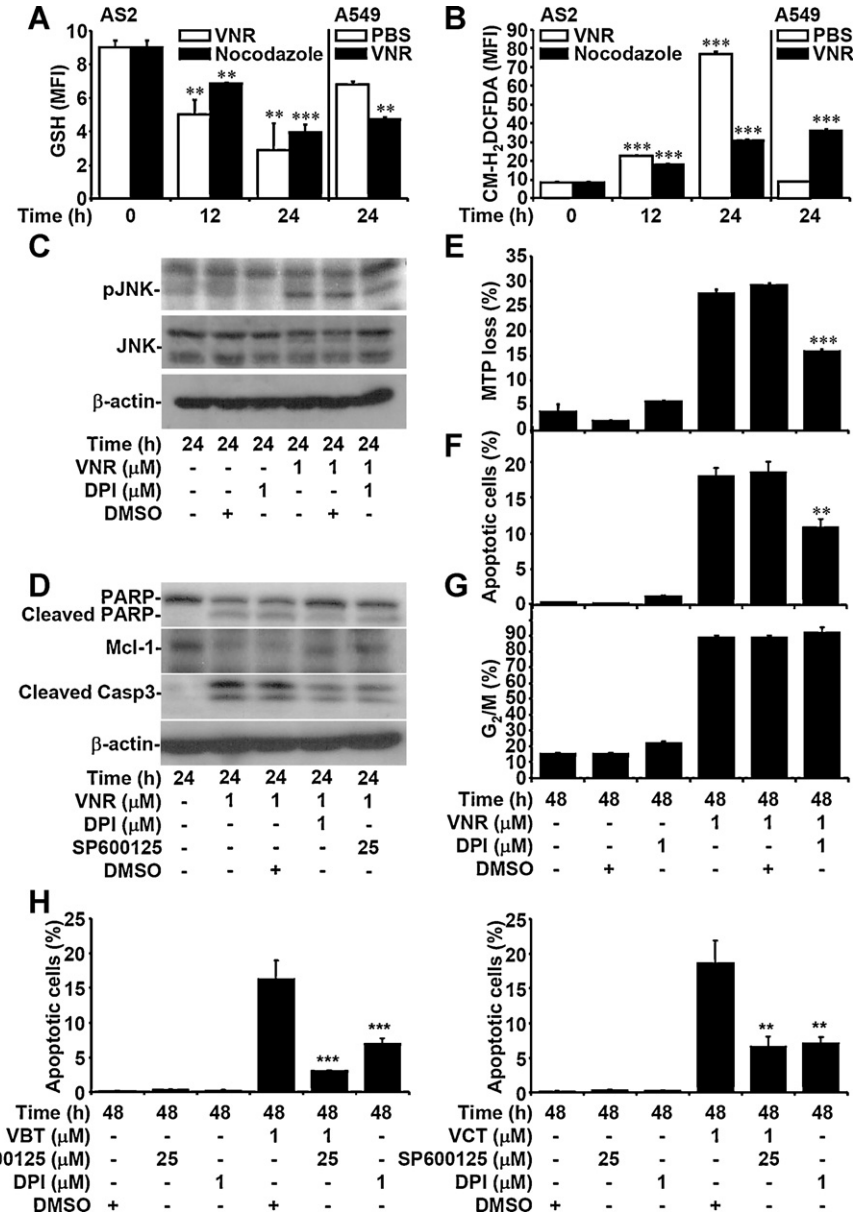

Fig. 6. ROS determines vinca alkaloid-induced JNK activation, Mcl-1 destabilization, MTP loss, caspase-3 activation, and cell apoptosis. The GSH Detection kit and CM-H_2DCFDA staining followed by flow cytometric analysis were used to determine the levels of GSH (A) and ROS (B), respectively, in VNR (1 μM)- or nocodazole (25 ng/ml)-treated AS2 and A549 cells for the indicated time. AS2 cells were pretreated with the antioxidant DPI or the JNK inhibitor SP600125 for 0.5 h followed by VNR, vinblastine (VBT), vincristine (VCT), or PBS treatment. Western blotting was used to determine the expression of phospho-JNK Thr183/Tyr185 (pJNK), JNK (C), PARP, Mcl-1, and cleaved caspase-3 (Casp3). β-actin was used as an internal control. One representative dataset obtained from repeated experiments is shown. Furthermore, rhodamine 123 and PI staining followed by flow cytometric analysis was used to determine the induction of MTP loss (E), cell apoptosis (F and H), and G_2/M phase arrest (G). DMSO was used as a negative control. For flow cytometric analyses, the percentages and MFI are the means ± SD of three individual experiments; $^{**}P < 0.01$ and $^{***}P < 0.001$, compared with the PBS-, VNR-, VBT-, or VCT-treated group.

an accumulation of ROS-generating mitochondria in cells under G_2/M phase arrest.

We next examined whether VNR caused mitochondrial dysfunction following aberrant ROS/JNK signaling. We previously demonstrated that VNR caused the loss of MTP, a hallmark of mitochondrial dysfunction (Fig. 3A). For cellular bioenergetic measurement, we used XF Extracellular Flux Analyzers to determine VNR-induced mitochondrial toxicity by monitoring OCR and ECAR [19]. Treatment of VNR profoundly inhibited OCR (Fig. 8A) following a compensatory increase in ECAR (Fig. 8B). Notably, inhibiting JNK by SP600125 treatment significantly ($P < 0.05$) reduced the VNR-induced imbalance of OCR/ECAR. These results demonstrate that VNR causes aberrant JNK-mediated mitochondrial dysfunction.

3.6. Involvement of JNK in VNR-induced DNA damage

Mitotic arrest usually causes DNA damage [26]; however, there is no evidence that VNR causes DNA damage-associated cellular cytotoxicity. Unexpectedly, immunostaining of γ-H2AX followed by flow cytometric analysis demonstrated that both VNR and nocodazole caused DNA damage in a JNK-regulated manner (Fig. 9A). This effect was inconsistent with cisplatin treatment, which causes DNA damage in any phase of the cell cycle, independent of JNK. Furthermore, immunostaining confirmed that both VNR and nocodazole induced γ-H2AX expression in AS2 cells via MPM2 expression or JNK activation (Fig. 9B). Using a caffeine treatment to inhibit ATR/ATM, we further clarified that DNA damage-associated ATR/ATM did not facilitate VNR-induced

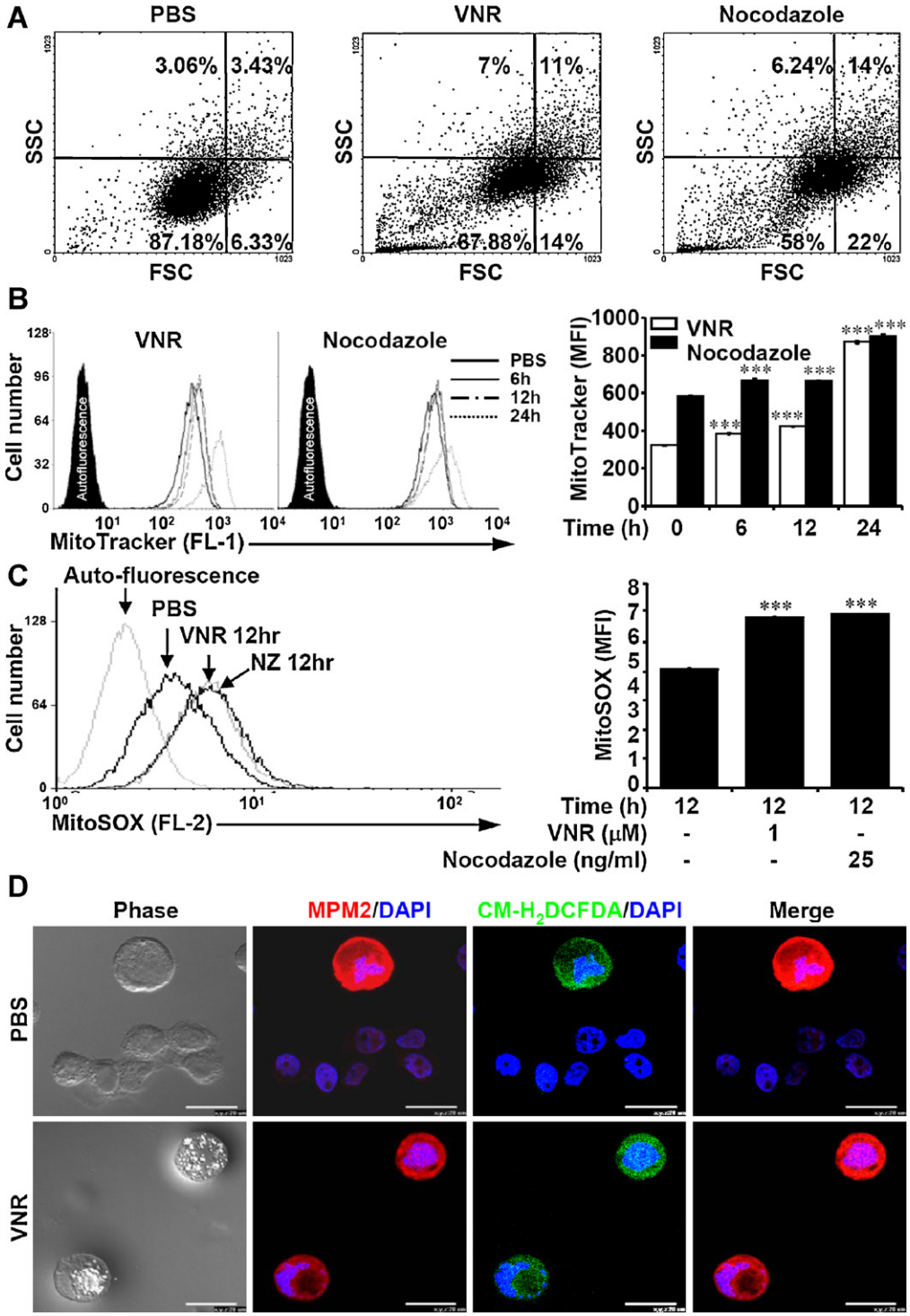

Fig. 7. VNR induces cell size change, mitochondrial accumulation, and ROS generation. (A) Flow cytometric analysis of AS2 cells treated with PBS, VNR (1 μM), or nocodazole (25 ng/ml) for 24 h. The scatter plot of forward scatter (FSC, X-scale) versus side scatter (SSC, Y-scale) indicates the cell size and granularity. (B) MitoTracker Green staining and flow cytometric analysis were used to detect mitochondrial expression in AS2 cells treated with PBS, VNR (1 μM), or nocodazole (25 ng/ml) for the indicated time. (C) MitoSOX staining and flow cytometric analysis were used to measure mitochondrial ROS generation. For flow cytometric analysis, one representative dataset obtained from repeated experiments is shown. The MFI is the means ± SD of three individual experiments; $^{***}P < 0.001$, compared with the PBS-treated group. (D) CM-H_2DCFDA plus MPM2 staining followed by fluorescent microscopic observations were used to determine ROS generation in mitotic phase cells without or with VNR (1 μM) treatment for 24 h. One representative image obtained from three individual experiments is shown. Scale bar is 25 μm.

G_2/M phase arrest (Fig. 9C) or apoptosis (Fig. 9D). These results show that VNR induces prolonged JNK activation followed by aberrant JNK-regulated DNA damage. VNR induces G_2/M phase arrest and apoptosis independently of DNA damage-associated ATR/ATM.

4. Discussion

To our knowledge, this is the first study to demonstrate a potent molecular mechanism for VNR cytotoxicity following an irreversible prometaphase arrest. Our findings, as summarized in Fig. 10,

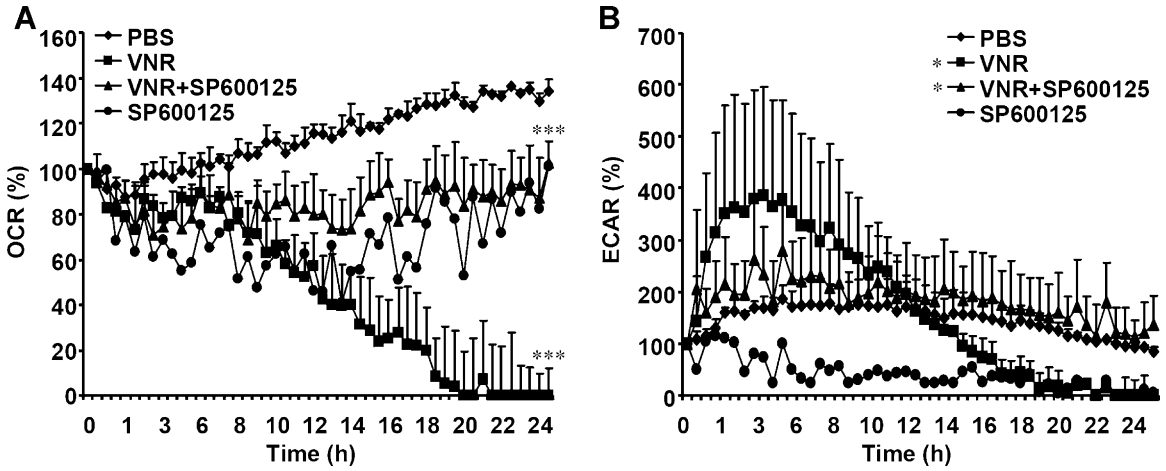

Fig. 8. JNK determines VNR-induced mitochondrial dysfunction. Seahorse BioScience technology was used to determine the levels of OCR (A) and ECAR (B) in VNR (1 μM)-treated AS2 cells for the indicated time. AS2 cells were pretreated with the JNK inhibitor SP600125 (25 μM) for 0.5 h followed by VNR or PBS treatment. After quantification of fluorescence intensity by the XF software algorithm, the levels of OCR and ECAR in PBS-treated group were normalized to 100%. The data are the means ± SD of three individual experiments; $^{*}P < 0.05$ and $^{***}P < 0.001$, compared with PBS- or VNR-treated group.

showed that mitotic inhibitors, such as vinca alkaloids and nocodazole, effectively caused ROS generation by increasing mitochondrial accumulation in lung adenocarcinoma cells. Aberrant ROS-mediated prolonged JNK activation induces DNA damage and Mcl-1 downregulation followed by mitochondrial dysfunction, caspase activation, and cell apoptosis. The signaling axis of the apoptotic pathway is not required for vinca alkaloids- and nocodazole-induced prometaphase arrest but is unusually activated following mitotic arrest. Consistent with a current study that has shown VNR induces ROS-mediated endothelial cell injury [4], we further provide the molecular mechanisms for ROS generation and ROS-regulated apoptotic signals in vinca alkaloid-treated lung adenocarcinoma cells.

For anticancer therapy, vinca alkaloid-induced G_2/M phase arrest was an indistinct concept for decades. However, in this study, immunostaining using an MPM2 antibody, which has been used to detect mitosis-specific and cell cycle controlled phosphoproteins such as DNA topoisomerase IIα and IIβ [20], we showed a specific prometaphase arrest caused by vinca alkaloids and nocodazole. Vinca alkaloids bind to the vinca-binding domain in the β-subunit of tubulin dimmers and then depolymerize microtubules by the destruction of mitotic spindles at high concentrations or block mitosis without depolymerization at low concentrations [27,28]. We showed evidence of mitotic prometaphase arrest due to the lack of α-tubulin rearrangement and the presence of lamin A/C degradation. Notably, mitotic arrest can be reversed at lower concentrations of VNR treatment (less than 5 nM) (Supplemental Fig. S2). Meanwhile, treatment with the reversible dose did not cause cell apoptosis. Clinically, the plasma concentration of VNR is decayed to 10 nM at 24 h after treatment using a previously reported therapeutic concentration of VNR [2,3].

The intrinsic pathway of apoptosis involves mitochondrial dysfunction, the release of cytochrome *c*, and activation of caspase-9 and caspase-3 [29,30]. Combining our results with previous studies [5,7], VNR causes apoptosis through the typical intrinsic pathway in lung adenocarcinoma cells. Furthermore, VNR causes apoptosis by decreasing Bcl-2 and Bcl-xL in lung carcinoma cells [8], while vinblastine induces inactivation of Bcl-2 and Bcl-xL in KB-3 carcinoma cells [14]. In addition to Bcl-2, we found that Mcl-1 expression was decreased. However, inhibition of GSK-3, proteasomes, and caspases, factors that regulate Mcl-1 stability [12,13], did not reverse Mcl-1 downregulation. The molecular basis for VNR-induced downregulation of Mcl-1 and Bcl-2 is therefore to be regulated through transcriptional as well as post-translational manners.

Activation of JNK is usually required for cell apoptosis [15]. Vinblastine and vincristine induced JNK activation in KB-3 cells [14]. Generally, JNK modulates pro- and anti-apoptotic proteins and facilitates death receptor-initiated extrinsic and mitochondrial intrinsic apoptotic pathways [31]. Both vinca alkaloids and nocodazole caused aberrant JNK-mediated mitochondrial dysfunction, while treatment with the JNK inhibitor SP600125 inhibited MTP loss, imbalance of OCR/ECAR, caspase activation, and cell apoptosis. It is noteworthy that VNR causes aberrant JNK-mediated Mcl-1 downregulation. Basically, JNK phosphorylates Mcl-1 and inactivates the function of Mcl-1 [32]. Our study, therefore, confers a pathway that links JNK-mediated Mcl-1 downregulation to vinca alkaloid-induced mitochondrial dysfunction. For apoptotic signaling, we found that VNR treatment caused JNK activation, accompanied by the activation of ASK1, a MAPK kinase kinase for JNK, under oxidative stress [33]. Notably, glutathione depletion and elevated ROS were demonstrated in VNR-treated endothelial cells [4]. To our knowledge, our findings are the first to demonstrate that VNR causes glutathione decrease and ROS increase in VNR-treated lung adenocarcinoma cells followed by ROS-mediated prolonged JNK activation, Mcl-1 downregulation, mitochondrial dysfunction, and cell apoptosis.

We found that vinca alkaloids and nocodazole caused prometaphase arrest, accompanied by the aberrant activation of ROS/JNK signaling. Actually, it is detectable but at minimal levels, allowing activated ROS/JNK signaling to positively co-stain within untreated mitotic cells under normal culture conditions. For cell cycle, JNK is important for the G_2/M transition; the inhibition of JNK causes G_2 phase arrest [34]. The mechanism underlying JNK activation during cell cycle progression is critical for exploring the critical processes of JNK-regulated cell cycle. In addition to MPM2, activated ROS/JNK signaling is specifically detectable for mitotic phase. Notably, the prolonged ROS/JNK activation has shown in VNR-stimulated cells. Furthermore, the involvement of ROS-regulated JNK is precluded for VNR-induced mitotic arrest but is productively activated following such an enlarged mitotic arrest. To study the mechanism by which VNR facilitates prolonged JNK activation following ROS generation, we noted the enlarged changes on cell size and granularity in either VNR- or nocodazole-treated cells. During the cell cycle, mitochondrial levels are increased for mitotic division [25]. Our findings indicate that either vinca alkaloids or nocodazole can cause prometaphase arrest,

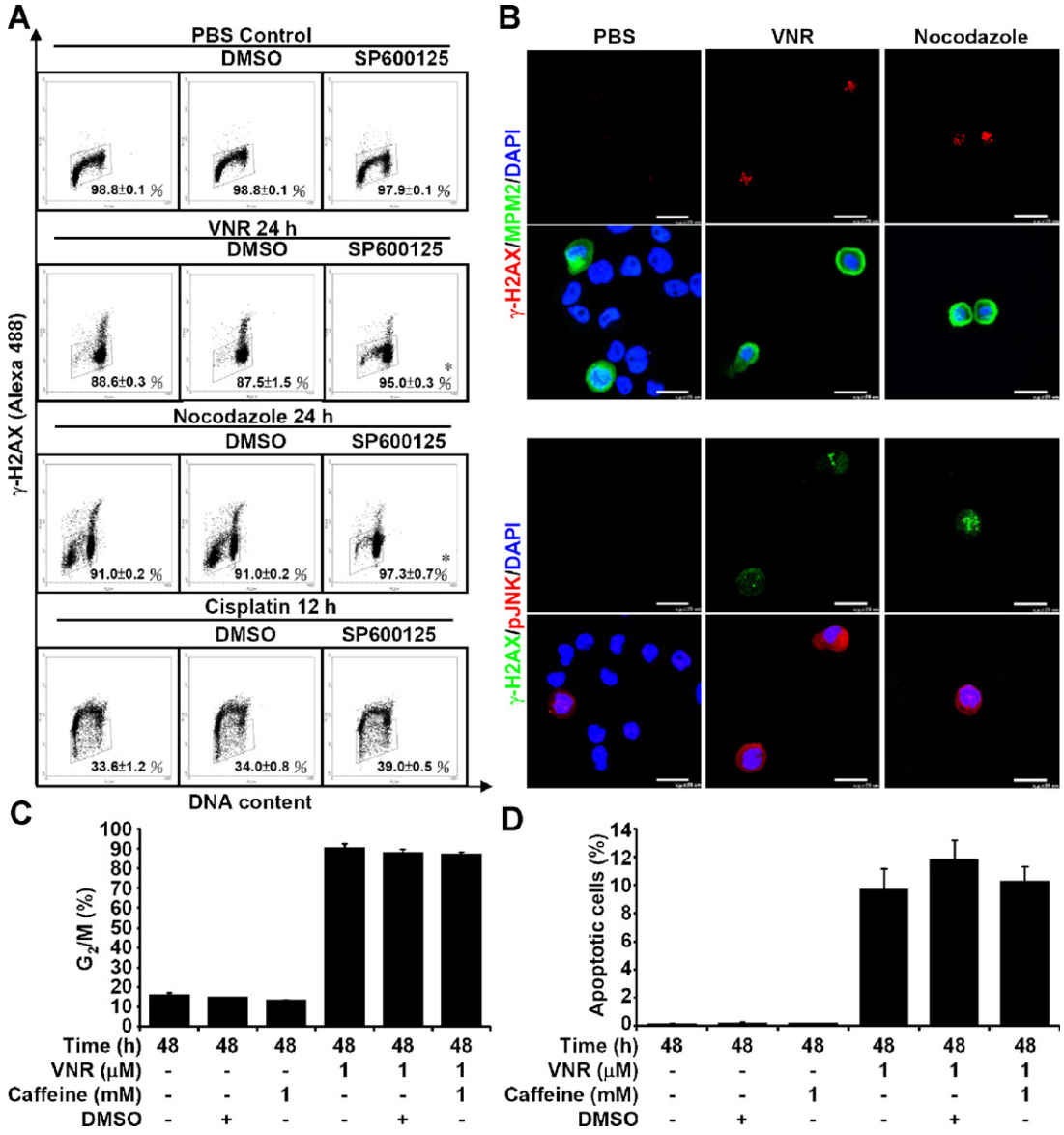

Fig. 9. Either VNR or nocodazole induces JNK-regulated DNA damage. γ-H2AX plus PI staining and flow cytometric analysis (A) or immunostaining of γ-H2AX plus MPM2 or phospho-JNK Thr183/Tyr185 (pJNK) and fluorescent microscopy (B) was used to detect DNA damage in AS2 cells treated with PBS, VNR (1 μM), or nocodazole (25 ng/ml) for 24 h. Cisplatin (50 ng/ml) and DMSO were used as the positive and negative controls, respectively. The data are the means ± SD of three individual experiments; $^*P < 0.05$, compared with VNR- or nocodazole-treated group. DAPI was used for nuclear staining. One representative dataset obtained from repeated experiments is shown. Scale bar is 25 μm. AS2 cells were pretreated with the ATR/ATM inhibitor caffeine for 0.5 h followed by VNR or PBS treatment. PI staining followed by flow cytometric analysis was used to determine the induction of G_2/M phase arrest (C) and cell apoptosis (D). DMSO was used as a negative control. The data are the means ± SD of three individual experiments.

which is accompanied by the accumulation of ROS-generating mitochondria during mitochondrial biogenesis. Basically, the mechanism of VNR-induced ROS generation is still unresolved in this study. According to our findings by MitoSOX staining, ROS-generating mitochondria are accumulated in VNR- and nocodazole-treated AS2 cells. While VNR rapidly caused ECAR increase, we speculate that ROS generation may be caused by VNR-induced mitochondria biogenesis followed by an increased ECAR. Based on these findings, mitochondrial ROS are the major sources of oxidative stress caused by VNR. Fortunately, under normal mitosis or during mitotic arrest caused by low concentrations of VNR treatment, the cells will complete the process of cell division or will be reversed from prometaphase arrest. In these cells, it is interesting to show whether ROS generation facilitates JNK activation to mediate the G_2/M transition. Furthermore, it is also possible that overdose treatment of vinca alkaloids or nocodazole could cause an irreversible and/or prolonged mitotic arrest that facilitates the accumulation of mitochondria, aberrant ROS generation, prolonged JNK activation, Mcl-1 downregulation, and mitochondrial dysfunction, including MTP loss and imbalance of OCR/ECAR.

In our study, VNR caused aberrant JNK-regulated DNA damage specifically in cells with mitotic arrest, as demonstrated by immunostaining using γH2AX antibody. This result was unexpected, compared to a previous study with cisplatin [35]. Previous studies showed that vincristine could induce DNA damage to promote apoptosis in human lymphocytes [36]. However, the effects of DNA damage on VNR-induced cell apoptosis are p53- and ATR/ATM-independent. Also, while JNK activation was not involved in VNR-induced M phase arrest, we precluded the involvement of JNK-regulated DNA damage for such effects. In the future study, the mechanism for VNR-induced DNA damage is noteworthy for further investigation. Basically, JNK may cause mitotic inhibition through DNA damage [37], p53/p21 signal

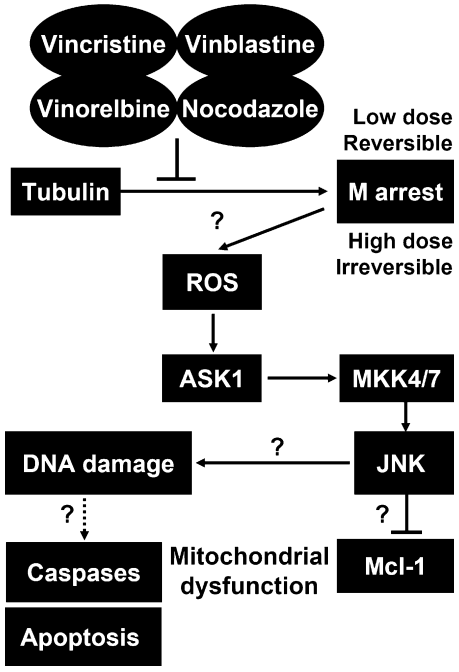

Fig. 10. Schematic model for vinca alkaloid-induced aberrant ROS/JNK-regulated cell apoptosis. After treatment with vinca alkaloids, cell growth was arrested at prometaphase due to the inhibition of microtubule polymerization. In these arrested cells, both vinca alkaloids and nocodazole induced accumulation of mitochondrial ROS to facilitate prolonged JNK activation accompanied by aberrant JNK-regulated DNA damage and JNK-regulated Mcl-1 downregulation followed by mitochondrial dysfunction, caspase activation, and cell apoptosis. Furthermore, these results show the molecular basis for potent vinca alkaloid-mediated anticancer activities.

transduction [38], or ATR/ATM activation [39]. Also, it is speculated that JNK causes DNA damage directly or indirectly through disrupting MTP followed then inducing AIF-mediated DNA damage [40,41]. However, according to our results, p53 and ATR/ATM are precluded for VNR-induced cytotoxicity because AS2 cells are loss of function of p53-mutated lung adenocarcinoma cells (Supplemental Fig. S3A) [42] and inhibiting ATR/ATM did not reduce VNR-induced cell apoptosis. To further clarify the involvement of p53 in VNR-induced mitotic arrest, p53 was silenced in A549 cells and results demonstrated that VNR caused G_2/M arrest in a p53-independent manner (Supplemental Fig. S3B).

In conclusion, our results explore a potent molecular mechanism for vinca alkaloid-induced cell apoptosis by sequentially inducing prometaphase arrest, ROS accumulation, prolonged JNK activation, DNA damage, Mcl-1 decrease, mitochondrial dysfunction, and caspase-mediated apoptosis. According to these findings, the anticancer mechanism of vinca alkaloids may take action by causing prometaphase arrest followed by cell apoptosis. Furthermore, part of these results may provide mechanistic details for combating cancer cells that have developed resistance to vinca alkaloids by interfering with ROS/JNK activation.

Acknowledgments

We thank the Immunobiology Core of the Research Center of Clinical Medicine at the National Cheng Kung University Hospital, College of Medicine, National Cheng Kung University, Tainan, Taiwan, for providing services that include training, technical support, and assistance with experimental design and data analysis using the Flow Cytometry Core facilities. This work was supported by grants NCKUH-9903028 and NCKUH-10003030 from the National Cheng Kung University Hospital in Taiwan and NSC 100-2320-B-006-009-MY3 from the National Science Council, Taiwan.

Appendix A. Supplementary data

Supplementary data associated with this article can be found, in the online version, at doi:10.1016/j.bcp.2012.01.016.

References

[1] Jemal A, Siegel R, Xu J, Ward E. Cancer statistics, 2010. CA Cancer J Clin 2010;60:277–300.
[2] Johnson SA, Harper P, Hortobagyi GN, Pouillart P. Vinorelbine: an overview. Cancer Treat Rev 1996;22:127–42.
[3] Gauvin A, Pinguet F, Poujol S, Astre C, Bressolle F. High-performance liquid chromatographic determination of vinorelbine in human plasma and blood: application to a pharmacokinetic study. J Chromatogr B Biomed Sci Appl 2000;748:389–99.
[4] Yamada T, Egashira N, Imuta M, Yano T, Yamauchi Y, Watanabe H, et al. Role of oxidative stress in vinorelbine-induced vascular endothelial cell injury. Free Radic Biol Med 2010;48:120–7.
[5] Toh HC, Sun L, Koh CH, Aw SE. Vinorelbine induces apoptosis and caspase-3 (CPP32) expression in leukemia and lymphoma cells: a comparison with vincristine. Leuk Lymphoma 1998;31:195–208.
[6] Goncalves A, Braguer D, Carles G, Andre N, Prevot C, Briand C. Caspase-8 activation independent of CD95/CD95-L interaction during paclitaxel-induced apoptosis in human colon cancer cells (HT29-D4). Biochem Pharmacol 2000;60:1579–84.
[7] Kosuke T. Short-term effects of preoperative administration of vinorelbine via the bronchial artery in non-small cell lung cancer patients. J Osaka Med Coll 2003;62:57–67.
[8] Sen S, Sharma H, Singh N. Curcumin enhances vinorelbine mediated apoptosis in NSCLC cells by the mitochondrial pathway. Biochem Biophys Res Commun 2005;331:1245–52.
[9] Hayakawa A, Kawamoto Y, Nakajima H, Sakai J, Takasawa R, Nakashima I, et al. Bid truncation mediated by caspases-3 and -9 in vinorelbine-induced apoptosis. Apoptosis 2008;13:523–30.
[10] Inoshita S, Takeda K, Hatai T, Terada Y, Sano M, Hata J, et al. Phosphorylation and inactivation of myeloid cell leukemia 1 by JNK in response to oxidative stress. J Biol Chem 2002;277:43730–4.
[11] Michels J, O'Neill JW, Dallman CL, Mouzakiti A, Habens F, Brimmell M, et al. Mcl-1 is required for Akata6 B-lymphoma cell survival and is converted to a cell death molecule by efficient caspase-mediated cleavage. Oncogene 2004;23:4818–27.
[12] Weng C, Li Y, Xu D, Shi Y, Tang H. Specific cleavage of Mcl-1 by caspase-3 in tumor necrosis factor-related apoptosis-inducing ligand (TRAIL)-induced apoptosis in Jurkat leukemia T cells. J Biol Chem 2005;280:10491–500.
[13] Maurer U, Charvet C, Wagman AS, Dejardin E, Green DR. Glycogen synthase kinase-3 regulates mitochondrial outer membrane permeabilization and apoptosis by destabilization of MCL-1. Mol Cell 2006;21:749–60.
[14] Stone AA, Chambers TC. Microtubule inhibitors elicit differential effects on MAP kinase (JNK, ERK, and p38) signaling pathways in human KB-3 carcinoma cells. Exp Cell Res 2000;254:110–9.
[15] Tobiume K, Matsuzawa A, Takahashi T, Nishitoh H, Morita K, Takeda K, et al. ASK1 is required for sustained activations of JNK/p38 MAP kinases and apoptosis. EMBO Rep 2001;2:222–8.
[16] Wang J, Yi J. Cancer cell killing via ROS: to increase or decrease, that is the question. Cancer Biol Ther 2008;7:1875–84.
[17] Yeh HH, Lai WW, Chen HH, Liu HS, Su WC. Autocrine IL-6-induced Stat3 activation contributes to the pathogenesis of lung adenocarcinoma and malignant pleural effusion. Oncogene 2006;25:4300–9.
[18] Lin CF, Chen CL, Chiang CW, Jan MS, Huang WC, Lin YS. GSK-3beta acts downstream of PP2A and the PI 3-kinase-Akt pathway, and upstream of caspase-2 in ceramide-induced mitochondrial apoptosis. J Cell Sci 2007;120:2935–43.
[19] Dykens JA, Jamieson JD, Marroquin LD, Nadanaciva S, Xu JJ, Dunn MC, et al. In vitro assessment of mitochondrial dysfunction and cytotoxicity of nefazodone, trazodone, and buspirone. Toxicol Sci 2008;103:335–45.
[20] Renzi L, Gersch MS, Campbell MS, Wu L, Osmani SA, Gorbsky GJ. MPM-2 antibody-reactive phosphorylations can be created in detergent-extracted cells by kinetochore-bound and soluble kinases. J Cell Sci 1997;110(Pt 17):2013–25.
[21] Hong FD, Chen J, Donovan S, Schneider N, Nisen PD. Taxol, vincristine or nocodazole induces lethality in G1-checkpoint-defective human astrocytoma U373MG cells by triggering hyperploid progression. Carcinogenesis 1999;20:1161–8.
[22] Ferri KF, Kroemer G. Organelle-specific initiation of cell death pathways. Nat Cell Biol 2001;3:E255–63.
[23] Brunelle JK, Letai A. Control of mitochondrial apoptosis by the Bcl-2 family. J Cell Sci 2009;122:437–41.
[24] Lillig CH, Holmgren A. Thioredoxin and related molecules—from biology to health and disease. Antioxid Redox Signal 2007;9:25–47.
[25] Zanet J, Freije A, Ruiz M, Coulon V, Sanz JR, Chiesa J, et al. A mitosis block links active cell cycle with human epidermal differentiation and results in endoreplication. PLoS One 2010;5:e15701.
[26] Dalton WB, Nandan MO, Moore RT, Yang VW. Human cancer cells commonly acquire DNA damage during mitotic arrest. Cancer Res 2007;67:11487–92.

[27] Bai RL, Pettit GR, Hamel E. Binding of dolastatin 10 to tubulin at a distinct site for peptide antimitotic agents near the exchangeable nucleotide and vinca alkaloid sites. J Biol Chem 1990;265:17141–9.
[28] Jordan MA, Thrower D, Wilson L. Mechanism of inhibition of cell proliferation by vinca alkaloids. Cancer Res 1991;51:2212–22.
[29] Orrenius S, Zhivotovsky B, Nicotera P. Regulation of cell death: the calcium-apoptosis link. Nat Rev Mol Cell Biol 2003;4:552–65.
[30] Fariss MW, Chan CB, Patel M, Van Houten B, Orrenius S. Role of mitochondria in toxic oxidative stress. Mol Interv 2005;5:94–111.
[31] Dhanasekaran DN, Reddy EP. JNK signaling in apoptosis. Oncogene 2008;27:6245–51.
[32] Sanchez-Perez T, Ortiz-Ferron G, Lopez-Rivas A. Mitotic arrest and JNK-induced proteasomal degradation of FLIP and Mcl-1 are key events in the sensitization of breast tumor cells to TRAIL by antimicrotubule agents. Cell Death Differ 2010;17:883–94.
[33] Ichijo H, Nishida E, Irie K, ten Dijke P, Saitoh M, Moriguchi T, et al. Induction of apoptosis by ASK1, a mammalian MAPKKK that activates SAPK/JNK and p38 signaling pathways. Science 1997;275:90–4.
[34] Oktay K, Buyuk E, Oktem O, Oktay M, Giancotti FG. The c-Jun N-terminal kinase JNK functions upstream of Aurora B to promote entry into mitosis. Cell Cycle 2008;7:533–41.
[35] Podhorecka M, Skladanowski A, Bozko P. H2AX phosphorylation: its role in DNA damage response and cancer therapy. J Nucleic Acids 2010;2010. doi:10.4061/2010/920161. pii: 920161.
[36] Jiang W, Lu Y, Chen Z, Chen S, Zhang M, Jin L, et al. Studying the genotoxicity of vincristine on human lymphocytes using comet assay, micronucleus assay and TCR gene mutation test in vitro. Toxicology 2008;252:113–7.
[37] Ho CY, Li HY. DNA damage during mitosis invokes a JNK-mediated stress response that leads to cell death. J Cell Biochem 2010;110:725–31.
[38] Garner E, Raj K. Protective mechanisms of p53-p21-pRb proteins against DNA damage-induced cell death. Cell Cycle 2008;7:277–82.
[39] Yang J, Xu ZP, Huang Y, Hamrick HE, Duerksen-Hughes PJ, Yu YN. ATM and ATR: sensing DNA damage. World J Gastroenterol 2004;10:155–60.
[40] Saelens X, Festjens N, Vande Walle L, van Gurp M, van Loo G, Vandenabeele P. Toxic proteins released from mitochondria in cell death. Oncogene 2004;23:2861–74.
[41] Kim R, Emi M, Tanabe K. Role of mitochondria as the gardens of cell death. Cancer Chemother Pharmacol 2006;57:545–53.
[42] Murai Y, Hayashi S, Takahashi H, Tsuneyama K, Takano Y. Correlation between DNA alterations and p53 and p16 protein expression in cancer cell lines. Pathol Res Pract 2005;201:109–15.